Syntheses, Structure, Magnetism, and Optical Properties of the Ordered Interlanthanide Copper Chalcogenides Ln_2YbCuQ_5 (Ln = La, Ce, Pr, Nd, Sm; Q = S, Se): Evidence for Unusual Magnetic Ordering in Sm_2YbCuS_5

Geng Bang Jin,[†] Eun Sang Choi,[‡] Robert P. Guertin,[§] Corwin H. Booth,[£]

and Thomas E. Albrecht-Schmitt[†,*]

[†]Department of Chemistry and Biochemistry and Center for Actinide Science, Auburn University, Auburn, Alabama 36849

[‡]Department of Physics and National High Magnetic Field Laboratory, Florida State University, Tallahassee, Florida 32310

[§]Department of Physics and Astronomy, Tufts University, Medford, Massachusetts 02155

[£]Chemical Sciences Division, Lawrence Berkeley National Laboratory, 1 Cyclotron Rd., Berkeley, CA 94720

A Submission to Inorganic Chemistry

Abstract

Ln_2YbCuQ_5 (Ln = La, Ce, Pr, Nd, Sm; Q = S, Se) have been prepared by direct reaction of the elements in Sb_2Q_3 (Q = S, Se) fluxes at 900 °C. All compounds have been characterized by single-crystal X-ray diffraction methods and they are isotypic. The structure of Ln_2YbCuQ_5 consists of one-dimensional $^{1}_{\infty}[YbCuQ_5]^{6-}$ ribbons extending along the *b* axis that are connected by larger Ln^{3+} ions. Each ribbon is constructed from two single chains of $[YbQ_6]$ octahedra with one double chain of $[CuQ_5]$ trigonal bipyramids in the middle. All three chains connect with each other via edge-sharing. There are two crystallographically unique Ln atoms, one octahedral Yb site, and two disordered Cu positions inside of distorted Q_5 trigonal bipyramids. Both Ln atoms are surrounded by eight Q atoms in bicapped trigonal prisms. The magnetic properties of Ln_2YbCuQ_5 have been characterized using magnetic susceptibility and heat capacity measurements, while their optical properties have been explored using UV-vis-NIR diffuse reflectance spectroscopy. $Ce_2YbCuSe_5$, La_2YbCuS_5, Ce_2YbCuS_5, and Pr_2YbCuS_5 are Curie-Weiss paramagnets. $La_2YbCuSe_5$ and Nd_2YbCuS_5 show evidence for short-range antiferromagnetic ordering at low temperatures. Sm_2YbCuS_5 shows magnetic ordering at 5.9 K, followed by negative magnetization at low external fields. The band gaps of $La_2YbCuSe_5$, $Ce_2YbCuSe_5$, La_2YbCuS_5, Ce_2YbCuS_5, Pr_2YbCuS_5, Nd_2YbCuS_5, and Sm_2YbCuS_5 are 1.15 eV, 1.05 eV, 1.45 eV, 1.37 eV, 1.25 eV, 1.35 eV, and 1.28 eV respectively.

Introduction

Rare-earth copper chalcogenides have been the source of considerable interest not only because of their diverse structures and electronic properties, but also because of some unusual coordination geometries and oxidation states of copper that they exhibit.[1-39] The large number of rare-earth copper chalcogenides can be divided into two groups based on different interactions between chalcogenides. In group one phases, there are no Q-Q (Q = S, Se, Te) interactions. These compounds have been generally synthesized at relatively high temperatures as thermodynamically stable products, which include $LnCuQ_2$ (Ln = rare-earth; Q = S, Se, Te),[1-11] $Ln_{0.66}Cu_2S_2$ (Ln = Gd, Er),[12-15] and Eu_2CuQ_3 (Q = S, Se).[16-18] $LnCuQ_2$ compounds adopt at least three different structures (monoclinic, orthorhombic, and trigonal) depending on the relative size of the Ln ions.[1-11] Mixed-valent Eu_2CuQ_3 phases have Eu^{2+} and Eu^{3+} ions occupying two crystallographically independently sites, and Eu_2CuS_3[17] shows a ferromagnetic transition at 3.4 K owing to the coupling of Eu^{2+} ions. Group two compounds contain polychalcogenide anions with various degrees of Q-Q interactions, which are considered as kinetic products. These compounds have been typically prepared using alkali-metal/lanthanide halide fluxes or reactive fluxes, thereby allowing for lower reaction temperatures. Examples include La_2CuS_4,[20] Sm_3CuSe_6,[21,22] $EuCu_{0.66}Te_2$,[23] $Gd_3Cu_2Te_7$,[24] $LaCu_{0.28}Te_2$,[25] and $LnCu_xTe_2$ (Ln = La, Nd, Sm, Gd and Dy).[26] La_2CuS_4 features unusual discrete $[S_3Cu\cdots S\text{-}S\cdots CuS_3]^{12-}$ units, which contain two nearly planar $[CuS_3]^{5-}$ triangles bridged by a disulfide anion. $EuCu_{0.66}Te_2$ contains a flat square net of Te atoms, while all of the latter three have linear Te chains.

Partial substitutions of chalcogenides have been tried to access new phases with different physical properties from the parent ternary phase $LnCuQ_2$, e.g. LaCuSTe[27] and SmCuSTe.[27] Lanthanide copper oxychalcogenides including LnCuOQ (Ln = La, Ce, Pr, Nd; Q = S, Se, Te),[28-38] $La_5Cu_6O_4S_7$,[39] and $La_3CuO_2S_3$[40] have been extensively studied. LnCuOQ adopt a structure with alternately stacking PbO-like $[Cu_2Q_2]^{2-}$ layers and anti-PbO-like $[Ln_2O_2]^{2+}$ layers, which is similar to that of copper-based high-T_c superconducting oxides.[28-38] LaCuOQ are wide band gap *p*-type semiconductors, and are considered as potential transparent conductive materials.[28-38] In contrast, $La_5Cu_6O_4S_7$ is metallic, and the average oxidation state of the Cu atoms is +7/6.[39]

A different approach to prepare new quaternary rare-earth copper chalcogenides is to partially replace the heavy metal in known ternary phases with different rare-earth elements. To our knowledge, $EuLnCuS_3$ (Ln = Y, Gd-Lu) [19] are the only known examples of interlanthanide copper chalcogenides, which were made by replacing the Eu^{3+} ions in Eu_2CuS_3 using other trivalent Ln atoms. The purpose of this study is to prepare new ordered quaternary interlanthanide copper chalcogenides phases by including two Ln atoms from opposite ends of the lanthanide series, which tend to have different coordination geometries in same compounds. Here we present the syntheses, structure, optical, magnetic, and heat capacity measurements of the new quaternary interlanthanide copper chalcogenides, Ln_2YbCuQ_5 (Ln = La, Ce, Pr, Nd, Sm; Q = S, Se).

Experimental

Starting Materials. La (99.9%, Alfa-Aesar), Ce (99.9%, Alfa-Aesar), Pr (99.9%, Alfa-Aesar), Nd (99.9%, Alfa-Aesar), Sm (99.9%, Alfa-Aesar), Yb (99.9%, Alfa-Aesar),

Cu (99%, Alfa-Aesar), S (99.5%, Alfa-Aesar), Se (99.5%, Alfa-Aesar), and Sb (99.5%, Alfa-Aesar) were used as received. The Sb_2Q_3 (Q = S, Se) fluxes were prepared from the direct reaction of the elements in sealed fused-silica ampoules at 850 °C.

Syntheses. Ln_2YbCuQ_5 (Ln = La, Ce, Pr, Nd, Sm; Q = S, Se) were prepared using Sb_2Q_3 (Q = S, Se) fluxes. 150 mg of Ln, Yb, Cu, and Q were stoichiometrically mixed with 75 mg of Sb_2Q_3 in fused-silica ampoules in an Ar-filled glovebox. The ampoules were sealed under vacuum and placed in a programmable tube furnace. The following heating profile was used: 2 °C/min to 500 °C (held for 1 h), 0.5 °C/min to 900 °C (held for 7 d), 0.04 °C/min to 500 °C (held for 2 d), and 0.5 °C/min to 24 °C. In each reaction the major phases included high yields of black crystals of desired products and unreacted Sb_2Q_3 lying in the bottom of the ampoules. This separation was achieved by slightly tilting the furnaces. Powder X-ray diffraction measurements were used to confirm phase purity by comparing the powder patterns calculated from the single-crystal X-ray structures with the experimental data. Semi-quantitative SEM/EDX analyses were performed using JEOL 840/Link Isis or JEOL JSM-7000F instruments. Ln, Yb, Cu, and Q percentages were calibrated against standards. Sb was not detected in the crystals. The Ln:Yb:Cu:Q ratios were determined to be approximately 2:1:1:5 from EDX analyses.

Crystallographic Studies. Single crystals of Ln_2YbCuQ_5 (Ln = La, Ce, Pr, Nd, Sm; Q = S, Se) were mounted on glass fibers with epoxy and optically aligned on a Bruker APEX single crystal X-ray diffractometer using a digital camera. Initial intensity measurements were performed using graphite monochromated Mo Kα (λ = 0.71073 Å) radiation from a sealed tube and monocapillary collimator. SMART (v 5.624) was used for preliminary determination of the cell constants and data collection control. The

intensities of reflections of a sphere were collected by a combination of 3 sets of exposures (frames). Each set had a different ϕ angle for the crystal and each exposure covered a range of 0.3° in ω. A total of 1800 frames were collected with exposure times per frame of 10 or 20 seconds depending on the crystal.

For Ln_2YbCuQ_5, determination of integrated intensities and global refinement were performed with the Bruker SAINT (v 6.02) software package using a narrow-frame integration algorithm. These data were treated first with a face-indexed numerical absorption correction using XPREP,[41] followed by a semi-empirical absorption correction using SADABS.[42] The program suite SHELXTL (v 6.12) was used for space group determination (XPREP), direct methods structure solution (XS), and least-squares refinement (XL).[41] The final refinements included anisotropic displacement parameters for all atoms and secondary extinction. Some crystallographic details are given in Table 1. As an example, atomic coordinates and equivalent isotropic displacement parameters for La_2YbCuS_5 are given in Table 2. Additional crystallographic details can be found in the Supporting Information.

Powder X-ray Diffraction. Powder X-ray diffraction patterns were collected with a Rigaku Miniflex powder X-ray diffractometer using Cu Kα (λ = 1.54056 Å) radiation.

Magnetic Susceptibility Measurements. Magnetic data were measured on Ln_2YbCuQ_5 (Ln = La, Ce, Pr, Nd, Sm; Q = S, Se) powders in gelcap sample holders with a Quantum Design MPMS magnetometer/susceptometer between 2 and 300 K and in applied fields up to 7 T. DC susceptibility measurements were made under zero-field-cooled conditions with an applied field of 0.1 T. Susceptibility values were corrected for

the sample diamagnetic contribution according to Pascal's constants[43] as well as for the sample holder diamagnetism. Weiss temperatures, θ_p, were obtained from extrapolations from fits between 100 and 300 K.

The heat capacity measurement was done for Sm_2YbCuS_5 using a Quantum Design PPMS. The powder sample was mixed with N grease as binding material, whose contribution to the total heat capacity was measured before the sample was mounted.

UV-vis-NIR Diffuse Reflectance Spectroscopy. The diffuse reflectance spectra for Ln_2YbCuQ_5 (Ln = La, Ce, Pr, Nd, Sm; Q = S, Se) were measured from 200 to 2500 nm using a Shimadzu UV3100 spectrophotometer equipped with an integrating sphere attachment. The Kubelka-Munk function was used to convert diffuse reflectance data to absorption spectra.[44]

Results and Discussion

Structures of Ln_2YbCuQ_5 (Ln = La, Ce, Pr, Nd, Sm; Q = S, Se). The compounds Ln_2YbCuQ_5 (Ln = La, Ce, Pr, Nd, Sm; Q = S, Se) are isotypic, and crystallize in the centrosymmetric, orthorhombic, space group *Pnma*. As illustrated in Figure 1, the structure can be described as composed of one-dimensional $^1_\infty[YbCuQ_5]^{6-}$ ribbons running down the [010] direction that are separated by Ln^{3+} ions. It includes two crystallographically unique Ln atoms, one octahedral Yb site, and two Cu positions. The polyhedra of Ln and Cu atoms are shown in Figure 2. Both Ln^{3+} cations are eight-coordinate and occur as bicapped trigonal prisms. The bond distances of LnQ_8 and YbQ_6 for Ln_2YbCuQ_5 are normal (See Supporting Information Table S1). For example, in the case of La_2YbCuS_5, La-S distances range from 2.9046(16) Å to 3.241(2) Å, and Yb-S

distances are in the range of 2.6311(16) Å to 2.7989(17) Å. These bond lengths are comparable to the sum of the ionic radii,[45] 3.00 Å for LaS_8 and 2.70 Å for YbS_6. Two Cu atoms are very close to each other with the Cu(1)-Cu(2) distance being 0.841(3) Å in case of La_2YbCuS_5. Obviously, these two sites cannot be occupied simultaneously. The occupancy of Cu(1) ranges from 0.19 to 0.54. Each Cu has a highly distorted tetrahedral environment. For example, the four Cu(1)-S distances for La_2YbCuS_5 are 2.257(3) Å, 2.3464(18) Å, 2.3464(18) Å, and 2.544(4) Å, and S-Cu(1)-S angles are in the range of 90.78(11)-116.16(8)°. These bond distances are closer to the average values for Cu with triangular coordination (e.g. 2.33 Å in Cu_2S[46,47]) than the ones for Cu with tetrahedral coordination (2.44 Å, according to Shannon[45]). Since there are no Q-Q bonds and Cu-Cu interactions, the oxidation states for each atom in Ln_2YbCuQ_5 can be assigned as +3/+3/+1/-2, respectively.

Similar coordination environments for Cu atoms in the structure of Ln_2YbCuQ_5 have been found in other lanthanide copper chalcogenides. Examples include Sm_3CuSe_6,[21,22] $Gd_3Cu_2Te_7$,[24] $LaCu_{0.28}Te_2$,[25] and $LnCu_xTe_2$ (Ln = La, Nd, Sm, Gd and Dy),[26] in which two disordered Cu sites are equivalent and the tetrahedra are less distorted. In order to better describe the connectivity among the polyhedra, Cu(1) and Cu(2) atoms can be considered as one average Cu site sitting in the cavities of a distorted trigonal bipyramid, as shown in Figure 2. The one dimensional $^1_\infty[YbCuQ_5]^{6-}$ ribbons, which are shown Figure 3a, consist of two single $[YbQ_6]$ octahedral chains with one double $[CuQ_5]$ trigonal bipyramidal chain in the middle. All three chains connect with each other via edge-sharing. Within the $[YbQ_6]$ octahedral chain, each unit shares edges with two neighbors along the chain direction, while each $[CuQ_5]$ trigonal bipyramid

shares corners along the *b* axis and shares edges with adjacent identical chains. The connectivity of [CuQ_5] trigonal bipyramids in these compounds is quite different from other known examples. For $Gd_3Cu_2Te_7$,[24] the [$CuTe_5$] trigonal bipyramids share corners with four [$CuTe_4$] tetrahedra within two-dimensional [Cu_2Te_5] layers (Figure 3b). In Figure 3c, [$CuSe_5$] trigonal bipyramids in Sm_3CuSe_6[21] share edges to form one-dimensional single chains along the [010] direction, while Figure 3d shows a two-dimensional [Cu_xTe_2] layer in $LaCu_{0.28}Te_2$[25] or $LnCu_xTe_2$ (Ln = La, Nd, Sm, Gd and Dy)[26], constructed from [$CuTe_5$] trigonal bipyramids sharing edges with four close neighbors and sharing corners with other four bipyramidal units.

It is noted that $La_3CuO_2S_3$[40] adopts a similar formula and the same space group as Ln_2YbCuQ_5;, however their structures are clearly different. In the structure of $La_3CuO_2S_3$, there are three eight-coordinate La^{3+} ions with bicapped trigonal prismatic geometry as illustrated in Figure 4. In contrast, the Yb ion in Ln_2YbCuQ_5 is only six-coordinated due to its smaller size. Furthermore the structure of $La_3CuO_2S_3$ only has one four-coordinate Cu^+ site in a regular [CuS_4] tetrahedron, while there are two disordered Cu positions with highly distorted tetrahedral coordination in the structure of Ln_2YbCuQ_5.

Magnetic Susceptibility. The inverse molar Ln magnetic susceptibilities for Ln_2YbCuQ_5 (Ln = La, Ce, Pr, Nd; Q = S, Se) in the range of 2-300 K are shown in Figures 5-7. Table 3 presents the magnetic parameters determined from Curie-Weiss fits between 100 – 300 K. All six compounds show a deviation from the Curie-Weiss law around 70 K, as indicated by the moderately large and negative Weiss temperatures, due either to a crystal field effect and/or anitferromagnetic interactions. There is no evidence of magnetic ordering for $Ce_2YbCuSe_5$, La_2YbCuS_5, Ce_2YbCuS_5, and Pr_2YbCuS_5. In

contrast, the magnetic susceptibilities for $La_2YbCuSe_5$ and Nd_2YbCuS_5 show changes in the slope at low temperature, which may indicate short-range antiferromagnetic ordering. The experimental effective magnetic moments per formula unit are very close to the theoretical values based on the free Ln^{3+} ions.

The low temperature magnetic properties of Sm_2YbCuS_5 show quite different behaviors from the other compounds. As shown in Figure 8, the high temperature inverse susceptibility looks similar to other compounds except for a more rapid decrease below 7 K. Subsequent detailed measurements around 7 K revealed anomalous behaviors especially at low fields. The results at representative fields are shown in Figure 9. The notable features are: (1) abrupt increase of susceptibility below 5.9 K; (2) upon further cooling, the susceptibility shows a field-dependent peak (5.7 K at 50 Oe, 5.3 K at 2 kOe) followed by negative susceptibility (magnetization reversal) at 50 and 100 Oe fields; and (3) for 1 kOe and 2 kOe, the susceptibility increases again with decreased temperatures. As the field increases, the anomalies become less significant and the susceptibility peak just below 5.9 K becomes a small bump at 70 kOe.

To identify the thermodynamic nature of these anomalies, we carried out heat capacity measurements and the results are shown in Figure 10. The λ-shape jump of the heat capacity suggests long range magnetic ordering in this material. The magnetic entropy change (ΔS) was determined through the relation $\Delta S = \int (C_p - C_{ph})/T \, dT$ where C_{ph} is the lattice contribution to the heat capacity. Using an empirical curve for the lattice contribution shown in Figure 10, we obtained ΔS=1.13 R (R = 8.31 J/K·mol). In the case of long range ordering of magnetic ions with total angular momentum J, ΔS is expressed as $\Delta S = R \ln (2J+1)$. The J values for the free ions give larger values of ΔS (J = 5/2, ΔS =

3.6 R for Sm^{3+}, J = 7/2, ΔS = 2.1 R for Yb^{3+}), presumably due to a CEF effect, consistent with the large negative Weiss temperature.

The abrupt increase of susceptibility data and λ-shape of the jump in the heat capacity at 5.9 K suggest a transition to long range magnetic order with finite magnetic moments aligned to the external field with T_c = 5.9 K. This kind of behavior was reported in $SmMnO_3$ compound, where antiferroamagnetic coupling between weak ferromagnetic Mn ions and paramagnetic Sm ions was ascribed to explain the temperature induced magnetization reversal.[48] Although we don't yet know the details of the magnetic ordering, it seems plausible that a similar situation exists here. In that case, from the temperature dependence of the susceptibility, it is more likely that only one of the ions is ferromagnetically ordered while the other ion is not ordered down to 1.8 K. Regardless, the intriguing temperature dependence at low fields may be understood by antiferromagnetic coupling between the two magnetic ions; one ferromagnetically ordered at below T_c while the moment of the other keeps increasing upon cooling. Since the polarization of the latter ion increases with cooling, the temperature induced magnetization reversal can occur below a certain temperature where the moments of the ions cancel each other due to antiferromagnetic coupling. At higher fields, the effect of the external field weakens the antiferromagnetic coupling strength, and then the magnetization is positive.

Optical Properties. The electronic structures of interlanthanide copper chalcogenides are expected to be different from the parent interlanthanide chalcogenides after introducing more soft and electronegative Cu^+ ions into the system. Cu^+ ions prefer to bind larger chalcogenides to form more covalent bonds. This is best exhibited by

LnCuOQ (Ln = La, Ce, Pr, Nd; Q = S, Se, Te) [28-38] series, which consists of alternately stacked $[Cu_2Q_2]^{2-}$ layers and $[Ln_2O_2]^{2+}$ layers. The optical properties of LnCuOQ (Ln = La, Pr, Nd; Q = S, Se, Te) are mainly determined by $[Cu_2Q_2]^{2-}$ layers, e.g. the valence band of LaCuOTe[38] is filled with Cu 3*d* and Te 5*p* states and the conduction band is composed of Cu 4*s*, Te 5*p* and La 5*d* states; La 4*f* states are well above the Fermi energy. LnCuOQ (Ln = La, Pr, Nd; Q = S, Se) are determined to be direct allowed p-type semiconductors with wide band gaps, while corresponding tellurides have indirect-type gaps.[35,38] In contrast, recent studies have shown that Ce 4*f* states in CeCuOS and $CeCu_{0.75}OS$ compounds are fully spin-polarized and delocalized, resulting in black colors and much smaller band gaps.[36] Another series of compounds with layered structures, $LnCuS_2$ (Ln = La, Nd, Sm, Gd, Dy, Ho, Yb, Lu, Y), are also wide band gap p-type semiconductors.[2] Substitution of larger chalcogenides narrows the band gaps by increasing the covalency in the Cu-Q bonds to lift the Fermi levels.[27,35]

The optical properties for Ln_2YbCuQ_5 (Ln = La, Ce, Pr, Nd, Sm; Q = S, Se) were measured by UV-vis-NIR diffuse reflectance spectroscopy. The spectra are presented in Figure 11. The band gaps of $La_2YbCuSe_5$, $Ce_2YbCuSe_5$, La_2YbCuS_5, Ce_2YbCuS_5, Pr_2YbCuS_5, Nd_2YbCuS_5, and Sm_2YbCuS_5 are determined to be 1.15 eV, 1.05 eV, 1.45 eV, 1.37 eV, 1.25 eV, 1.35 eV, and 1.28 eV, respectively. Apparently the selenides have smaller band gaps than the sulfides due to the higher energy of Se 4*p* orbitals. The two lanthanum compounds have somewhat larger values than the rest. This means 4*f* states of other lanthanides besides La have some contribution to the electronic structures around the Fermi levels. Ce_2YbCuS_5 has slightly larger values than the Pr, Nd, and Sm cases. This behavior is unusual for many lanthanide and interlanthanide chalcogenides series

due to the high energy of $4f^1$ electron of cerium.[49-52] The band structures of Ln_2YbCuS_5 are therefore more controlled by Cu energy levels, as expected, because of the more strongly covalent Cu-S bonds. The fine-structures in these spectra are 4f-4f transitions for the lanthanide ions.

The band gaps of Ln_2YbCuQ_5 are consistent with the observed black colors, and are reasonable compared to $SmCuS_2$ (2.1 eV)[6] and $La_3CuO_2S_3$ (2.01 eV)[40], which have less condensed structures and lower energy O 2*p* orbitals, respectively. Overall, the electronic structures of Ln_2YbCuQ_5 are potentially tunable based on the choices of Ln and Q.

Conclusions

A new series of ordered quaternary interlanthanide copper chalcogenides, Ln_2YbCuQ_5 (Ln = La, Ce, Pr, Nd, Sm; Q = S, Se), have been synthesized using Sb_2Q_3 (Q = S, Se) fluxes at 900 °C. Compared to other known lanthanide copper chalcogenides, these compounds crystallize in a new structure type that is realized by including two different lanthanides with a large ionic size difference, which tend to have distinct coordination environments. The three-dimensional complex structure of Ln_2YbCuQ_5 (Ln = La, Ce, Pr, Nd, Sm; Q = S, Se) includes two crystallographically unique eight-coordinate Ln atoms: one octahedral Yb site, and two Cu positions. These two Cu sites closely reside in the trigonal bipyramidal cavities formed by Q^{2-} anions that cannot be occupied simultaneously. The structure includes one-dimensional $[YbCuQ_5]^{6-}$ ribbons along the *b* axis that are separated by larger Ln^{3+} ions. $Ce_2YbCuSe_5$, La_2YbCuS_5, Ce_2YbCuS_5, and Pr_2YbCuS_5 are Curie-Weiss paramagnets. $La_2YbCuSe_5$ and Nd_2YbCuS_5

have short-range antiferromagnetic ordering at low temperature. Sm_2YbCuS_5 shows evidence of long-range magnetic ordering at 5.9 K with antiferromagnetic coupling between Sm^{3+} and Yb^{3+} ions. The UV-vis-NIR diffuse reflectance measurements show these compounds to be wide band-gap semiconductors.

Acknowledgment. This work was supported by the U.S. Department of Energy (DOE) under Grant DE-FG02-02ER45963 through the EPSCoR Program. Funds for purchasing the UV-vis-NIR spectrometer used in these studies were provided through the Chemical Sciences, Geosciences and Biosciences Division, Office of Basic Energy Sciences (OBES), Office of Science (OS), Heavy Elements Program, U.S. Department of Energy under Grant DE-FG02-01ER15187. ESC acknowledges support from NSF-DMR 0203532. CHB acknowledges support from by the Director, OS, OBES, of the U.S. DOE under Contract No. DE-AC02-05CH11231. A portion of this work was performed at the National High Magnetic Field Laboratory, which is supported by the National Science Foundation Cooperative Agreement No. DMR-0084173, by the State of Florida, and by the Department of Energy.

Supporting Information Available: X-ray crystallographic files in CIF format for Ln_2YbCuQ_5 (Ln = La, Ce, Pr, Nd, Sm; Q = S, Se). This material is available free of charge via the Internet at http://pubs.acs.org. Selected bond distances and angles for Ln_2YbCuQ_5 (Ln = La, Ce, Pr, Nd, Sm; Q = S, Se) are also available in a summary table (S1). Magnetization data for Ln_2YbCuQ_5 (Ln = La, Ce, Pr, Nd, Sm; Q = S, Se) are also provided.

References

1) Julien-Pouzol, M.; Jaulmes, S.; Mazurier, A.; Guittard, M. *Acta Crystallogr., Sect. B: Struct. Crystallogr. Cryst. Chem.* **1981**, *37*, 1901.

2) Murugesan, T.; Gopalakrishnan, J. *Indian J. Chem.* **1983**, *22A*, 469.

3) Guseinov, G. G.; Amirov, A. S.; Mamedov, K. S. *Dokl. Akad. Nauk Az. SSR* **1984**, *40*, 62.

4) Gschneidner, K. A., Jr., Eyring, L. R., Eds. *Handbook on the Physics and Chemistry of Rare Earths*; North-Holland Physics Publishing: New York, 1984; Vol. 6.

5) Wang, Yarong; Sato, Nobuaki; Fujino, Takeo *Mater. Res. Bull.* **2001**, *36*, 1029.

6) Llanos, Jaime; Mujica, Carlos; Sanchez, Victor; Schnelle, Walter; Cardoso-Gil, Raul. *J. Solid State Chem.* **2004**, *177*, 1388.

7) Ijjaali, I.; Mitchell, K.; Ibers, J. A. *J. Solid State Chem.* **2004**, *177*, 760.

8) Julien-Pouzol, M.; Guittard, M.; Mazurier, A. *C. R. Acad. Sci.* **1970**, *271*, 1317.

9) Julien-Pouzol, M.; Guittard, M. *Ann. Chim. (Paris)* **1972**, *7*, 253.

10) Lauxmann, Petra; Schleid, Thomas. *Z. Anorg. Allg. Chem.* 2000, 626, 1608.

11) Dismukes, J. P.; Smith, R. T.; White, J. G. *J. Phys. Chem. Solids* **1971**, *32*, 913.

12) Ballestracci, R.; Bertaut, E. F. *C. R. Acad. Sci. Paris* **1965**, *261*, 5064.

13) Ballestracci, R.; Bertaut, E. F. *Bull. Soc. Miner. Crystallogr.* **1965**, *88*, 575.

14) Guymont, M.; Thomas, A.; Julien-Pouzol, M.; Jaulmes, S.; Guittard, M. *Phys. Status Solidi A* **1990**, ***121***, 21.

15) Onoda, M.; Chen, X. A.; Sato, A.; Wada, H. *J. Solid State Chem.* **2000**, *152*, 332.

16) Lemoine, P.; Carré, D.; Guittard, M. *Acta Cryst.* **1986**, *C42*, 390.

17) Furuuchi, F.; Wakeshima, M.; Hinatsu, Y. *J. Solid State Chem.* **2004**, *177*, 3853.

18) Eu_2CuSe_3, isostructure to Eu_2CuS_3, unpublished results.

19) Wakeshima, M.; Furuuchi, F. Hinatsu, Y. *J. Phys.: Condens. Matter* **2004**, *16* 5503.

20) Strobel, S.; Schleid, T. *Angew. Chem. Int. Ed.* **2003**, *42*, 4911.

21) Strobel, S.; Schleid, T. *J. Solid State Chem.* **2003**, *171*, 424.

22) Ijjaali, I.; Ibers, J. A. *Acta Cryst.***2004**, *E39*, i89.

23) Patschke, R.; Brazis, P.; Kannewurf, C. R.; Kanatzidis, M. G. *J. Mater. Chem.* **1999**, *9*, 2293.

24) Huang, F. Q.; Ibers, J. A. *J. Solid State Chem.* **2001**, *159*, 186.

25) Dung, N.-H.; Pardo, M.-P.; Boy, P. *Acta Cryst.***1983**, *C39*, 668.

26) Huang, F. Q.; Brazis, P.; Kannewurf, C. R.; Ibers, J. A. *J. Am. Chem. Soc.* **2000**, *122*, 80.

27) Huang, F. Q.; Ibers, J. A. *Inorg. Chem.* **1999**, *38*, 5978.

28) Popovkin, B. A.; Kusainova, A. M.; Dolgikh, V. A.; Aksel'rud, L. G. *Russ. J. Inorg. Chem. (Transl. of Zh. Neorg. Khim.)* **1998**, *43*, 1471.

29) Charkin, D. O.; Akopyan, A. V.; Dolgikh, V. A. *Russ. J. Inorg. Chem. (Transl. of Zh. Neorg. Khim.)* **1999**, *44*, 833.

30) Ueda, K.; Inoue, S.; Hirose, S.; Kawazoe, H.; Hosono, H. *Appl. Phys. Lett.* **2000**, *77*, 2701.

31) Ueda, K.; Inoue, S.; Hosono, H.; Sarukura, N.; Hirano, H. *Appl. Phys. Lett.* **2001**, *78*, 2333.

32) Inoue, S.; Ueda, K.; Hosono, H.; Hamada, N. *Phys. Rev. B* **2001**, *64*, 245211.

33) Ueda, K.; Takafuji, K.; Hiramatsu, H.; Ohta, H.; Kamiya, T.; Hirano, M.; Hosono, H. *Chem. Mater.* **2003**, *15*, 3692.

34) Ueda, K.; Takafuji, K.; Hosono, H. *J. Solid State Chem.* **2003**, *170*, 182.

35) Ueda, K.; Hosono, H.; Hamada, N. *J. Phys.: Condens. Matter* **2004**, *16*, 5179.

36) Chan, G. H.; Deng, B.; Bertoni, M.; Ireland, J. R.; Hersam, M. C.; Mason, T. O.; Van Duyne, R. P.; Ibers, J. A. *Inorg. Chem.* **2006**, *45*, 8264.

37) Ueda, K.; Hiramatsu, H.; Hirano, M.; Kamiya, T.; Hosono, H. *Thin Solid Films* **2006**, *496*, 8.

38) Liu, M. L.; Wu, L. B.; Huang, F. Q.; Chen, L. D.; Ibers, J. A. *J. Solid State Chem.* **2007**, *180*, 62.

39) Huang, F. Q.; Brazis, P.; Kannewurf, C. R.; Ibers, J. A. *J. Solid State Chem.* **2000**, *155*, 366.

40) Ijjaali, I.; Haynes, C. L.; Mcfarland, A. D.; Van Duyne, R. P.; Ibers, J. A. *J. Solid State Chem.* **2003**, *172*, 257.

41) Sheldrick, G. M. SHELXTL PC, Version 6.12, An Integrated System for Solving, Refining, and Displaying Crystal Structures from Diffraction Data; Siemens Analytical X-Ray Instruments, Inc.: Madison, WI 2001.

42) Sheldrick, G. M. *SADABS* 2001, Program for absorption correction using SMART CCD based on the method of Blessing: Blessing, R. H. *Acta Crystallogr.* **1995**, *A51*, 33.

43) Mulay, L. N.; Boudreaux, E. A. *Theory and Applications of Molecular Diamagnetism*; Wiley–Interscience: New York, 1976.

44) Wendlandt, W. W.; Hecht, H. G.: *Reflectance Spectroscopy*. Interscience Publishers, New York, 1966.

45) Shannon, R. D. *Acta Cryst.***1976**, *A32*, 751.

46) Evans, H. T., Jr. *Nature* **1971**, *232*, 69.

47) Evans, H. T., Jr. *Z. Kristallogr*. **1979**, *150*, 299.

48) Ivanov, V. Y.; Mukhin, A. A.; Prokhorov, A. S.; Balbashov, A. M. *Phys. Stat. Sol. (b)* **2003**, *236*, 445.

49) Prokofiev, A. V.; Shelykh, A. I.; Golubkov, A. V.; Smirnov, I. A. *J. Alloys Compd.* **1995**, *219*, 172.

50) Prokofiev, A. V.; Shelykh, A. I.; Melekh, B. T. *J. Alloys Compd.* **1996**, *242*, 41.

51) Jin, G. B.; Choi, E. S.; Guertin, R. P.; Brooks, J. S.; Bray, T. H.; Booth, C. H.; Albrecht-Schmitt, T. E. *Chem. Mater.* **2007**, *19*, 567.

52) Jin, G. B.; Choi, E. S.; Guertin, R. P.; Brooks, J. S.; Bray, T. H.; Booth, C. H.; Albrecht-Schmitt, T. E. *J. Solid State Chem.* **2007**, *180*, 2129.

Table 1. Crystallographic Data for Ln_2YbCuQ_5 (Ln = La, Ce, Pr, Nd, Sm; Q = S, Se).

Formula	$La_2YbCuSe_5$	$Ce_2YbCuSe_5$	La_2YbCuS_5	Ce_2YbCuS_5	Pr_2YbCuS_5	Nd_2YbCuS_5	Sm_2YbCuS_5
fw	909.20	911.62	674.70	677.12	678.70	685.36	697.58
Color	black	black	black	black	black	black	black
Crystal System	orthorhombic	orthorhombic	orthorhombic	orthorhombic	orthorhombic	orthorhombic	orthorhombic
Space group	*Pnma* (No. 62)	*Pnma* (No. 62)	*Pnma* (No. 62)	*Pnma* (No. 62)	*Pnma* (No. 62)	*Pnma* (No. 62)	*Pnma* (No. 62)
a (Å)	12.1326(11)	12.1113(7)	11.615(4)	11.5616(13)	11.547(2)	11.5466(8)	11.5323(8)
b (Å)	4.1119(4)	4.0780(3)	3.9662(13)	3.9304(4)	3.9071(8)	3.8927(3)	3.8531(3)
c (Å)	17.6653(16)	17.5714(11)	16.923(6)	16.8423(18)	16.795(3)	16.7597(11)	16.6470(12)
V (Å^3)	881.29(14)	867.85(10)	779.6(5)	765.34(14)	757.7(3)	753.31(9)	739.71(9)
Z	4	4	4	4	4	4	4
T (K)	193	193	193	193	193	193	193
λ (Å)	0.71073	0.71073	0.71073	0.71073	0.71073	0.71073	0.71073
ρ_{calcd} (g cm^{-3})	6.853	6.977	5.748	5.877	5.950	6.043	6.264
μ (cm^{-1})	429.51	442.61	265.47	277.73	288.98	299.16	323.04
R(F)[a]	0.0369	0.0290	0.0261	0.0242	0.0317	0.0250	0.0263
$R_w(F_o^2)$ [b]	0.0966	0.0757	0.0628	0.0588	0.0736	0.0566	0.0665

[a] $R(F) = \sum \| F_o | - | F_c \| / \sum | F_o |$ for $F_o^2 > 2\sigma(F_o^2)$. [b] $R_w\left(F_o^2\right) = \left[\sum \left[w\left(F_o^2 - F_c^2\right)^2 \right] / \sum w F_o^4 \right]^{1/2}$.

Table 2. Atomic Coordinates and Equivalent Isotropic Displacement Parameters for La_2YbCuS_5.

Atom (site)	*x*	*y*	*z*	U_{eq} (Å^2)[a]	*Occupancy*
La(1)	0.97977(4)	-0.25	0.82545(3)	0.00691(14)	1
La(2)	0.86754(4)	0.25	0.40038(3)	0.00686(14)	1
Yb(1)	0.80240(3)	0.25	0.63683(2)	0.01060(13)	1
Cu(1)	0.6657(2)	-0.25	0.51632(13)	0.0144(4)	0.54
Cu(2)	0.5960(3)	-0.25	0.50288(17)	0.0177(6)	0.46
S(1)	1.01210(17)	0.25	0.69895(13)	0.0066(4)	1
S(2)	0.81356(17)	-0.75	0.88370(13)	0.0072(4)	1
S(3)	0.88403(18)	-0.25	0.53444(13)	0.0104(4)	1
S(4)	0.59555(18)	0.25	0.57265(13)	0.0084(4)	1
S(5)	0.73861(18)	-0.25	0.72916(13)	0.0076(4)	1

[a] U_{eq} is defined as one-third of the trace of the orthogonalized U_{ij} tensor.

Table 3. Magnetic Parameters for Ln_2YbCuQ_5 (Ln = La, Ce, Pr, Nd, Sm; Q = S, Se).

Formula	P_{cal}/μ_B	P_{eff}/μ_B	θ_p (K)	R^2
$La_2YbCuSe_5$	4.54	4.229(9)	-38(1)	0.99959
$Ce_2YbCuSe_5$	5.79	5.76(1)	-54(1)	0.99962
La_2YbCuS_5	4.54	4.372(6)	-68.4(8)	0.99981
Ce_2YbCuS_5	5.79	5.31(3)	-47(2)	0.99794
Pr_2YbCuS_5	6.80	7.00(2)	-44(2)	0.99926
Nd_2YbCuS_5	6.84	6.87(1)	-46.0(8)	0.99979
Sm_2YbCuS_5	4.69	4.8(7)	-74(5)	0.9996

[a] P_{cal} and P_{eff} : calculated and experimental effective magnetic moments per formula unit.
[b] Weiss temperature (θ_p) and goodness of fit (R^2) obtained from high temperature (100-300 K) data

Figure Captions

Figure 1. A view of the three-dimensional structure of La_2YbCuS_5 along the *b* axis. La-S bonds have been omitted for clarity.

Figure 2. Illustrations of the coordination environments for La and Cu ions in La_2YbCuS_5.

Figure 3. Depictions of various connectivities of $[CuQ_5]$ (Q = S, Se, Te) trigonal bipyramids in different compounds: a) La_2YbCuS_5; b) $Gd_3Cu_2Te_7$[24]; c) Sm_3CuSe_6[21]; d) $LaCu_{0.28}Te_2$[25].

Figure 4. Unit cell of $La_3CuO_2S_3$[40] viewed along the *b* axis.

Figure 5. Inverse molar magnetic susceptibility vs temperature between 2 and 300 K for La_2YbCuS_5, Ce_2YbCuS_5, and Pr_2YbCuS_5. Data were taken under an applied magnetic field of 0.1 T. The straight line represents the fit to Curie-Weiss law in the range of 100-300 K.

Figure 6. Inverse molar magnetic susceptibility vs temperature and fit for Nd_2YbCuS_5 as in Figure 5. Inset shows the inverse molar magnetic susceptibility at low temperature.

Figure 7. Inverse molar magnetic susceptibility vs temperature and fit $La_2YbCuSe_5$ and Ce_2YbCuS_5, as in Figure 5. Inset shows the inverse molar magnetic susceptibility for $La_2YbCuSe_5$ at low temperature.

Figure 8. Inverse molar magnetic susceptibility vs temperature and fit for Sm_2YbCuS_5, as in Figure 5. Inset shows the inverse molar magnetic susceptibility at low temperature.

Figure 9. Magnetic susceptibility data for Sm_2YbCuS_5 at low temperatures under external fields of (a) 50, 1000 Oe and (b) 0.5, 1, 2, 70 kOe. The external field was applied or removed at 30 K. For 70 kOe, the difference between ZFC and FC is negligible.

Figure 10. The temperature dependence of heat capacity of Sm_2YbCuS_5. The solid line is an empirical fitting curve of the lattice heat capacity (C_{ph}).

Figure 11. UV-vis diffuse reflectance spectra of Ln_2YbCuQ_5 (Ln = La, Ce, Pr, Nd, Sm; Q = S, Se).

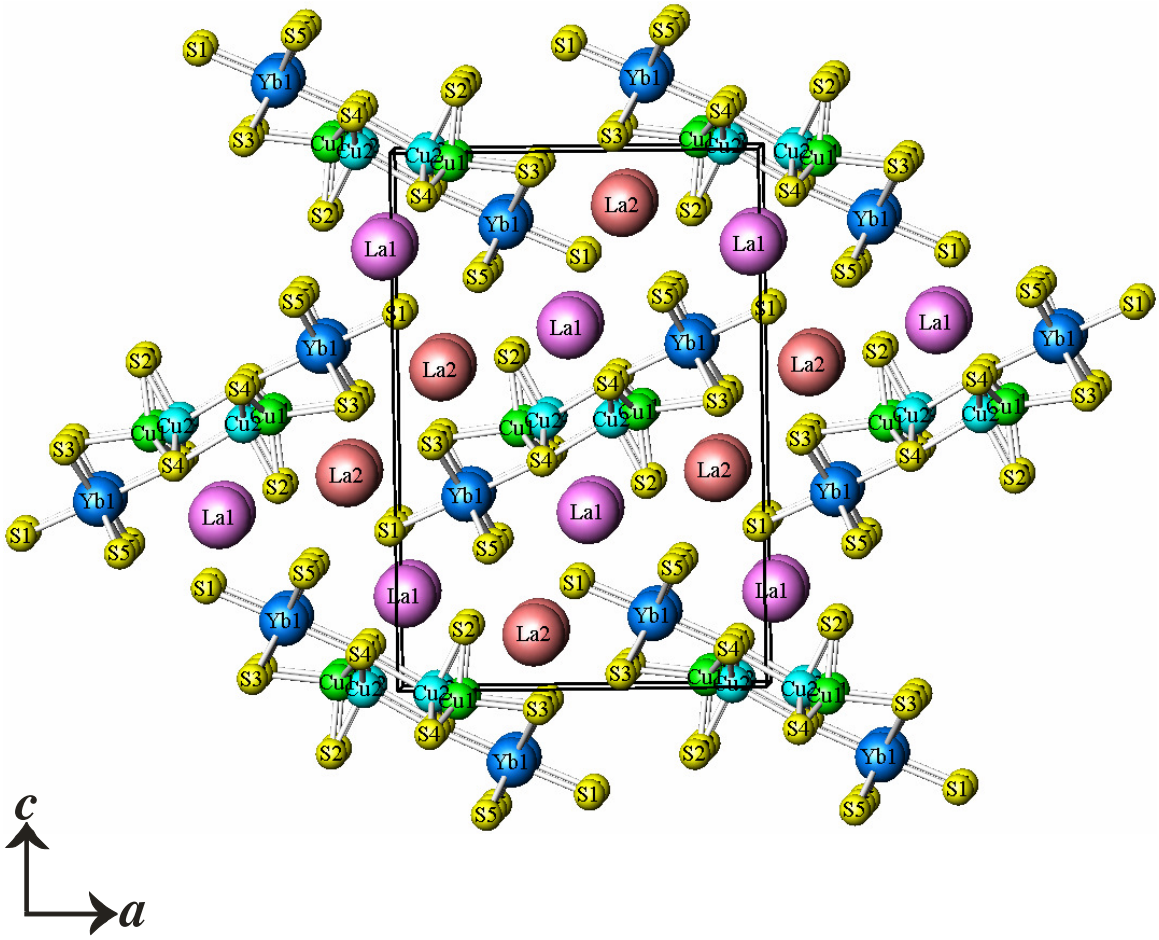

Figure 1

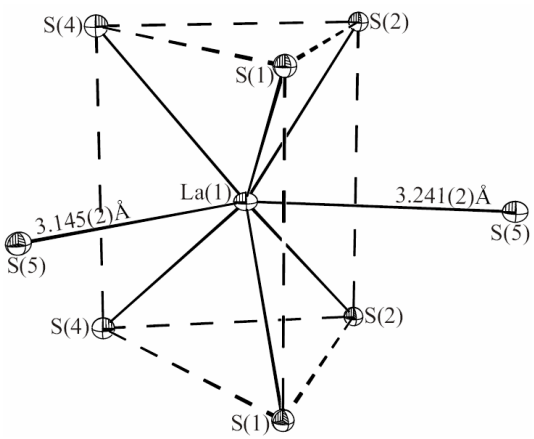
S(4)
S(2)
S(1)
La(1)
3.241(2)Å
3.145(2)Å
S(5)
S(5)
S(4)
S(2)
S(1)

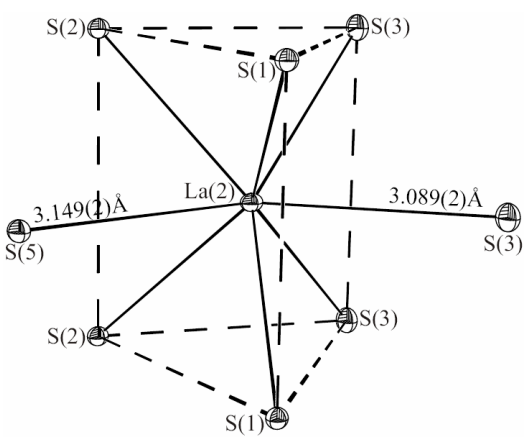
S(2)
S(3)
S(1)
La(2)
3.089(2)Å
3.149(2)Å
S(5)
S(3)
S(2)
S(3)
S(1)

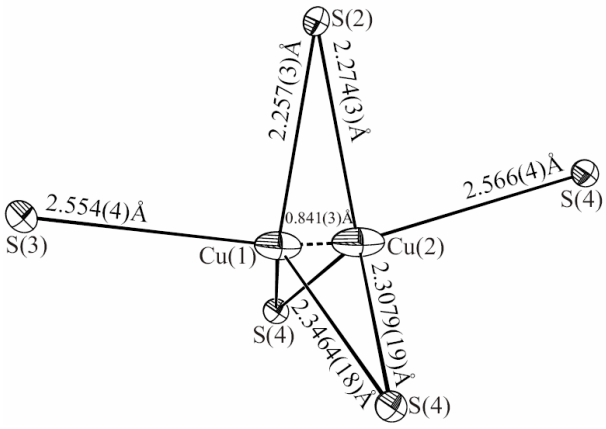
S(2)
2.257(3)Å
2.274(3)Å
2.566(4)Å
S(4)
2.554(4)Å
S(3)
0.841(3)Å
Cu(1)
Cu(2)
2.3079(19)Å
S(4)
2.3464(18)Å
S(4)

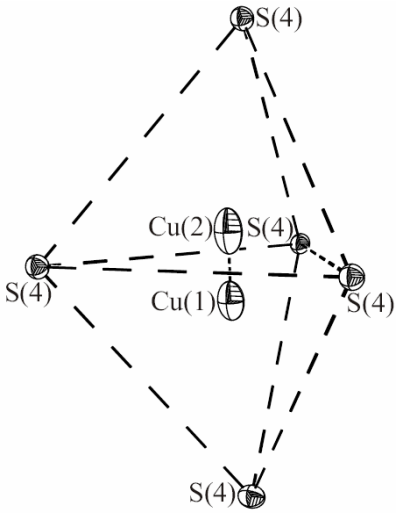
S(4)
Cu(2)
S(4)
S(4)
Cu(1)
S(4)
S(4)

Figure 2

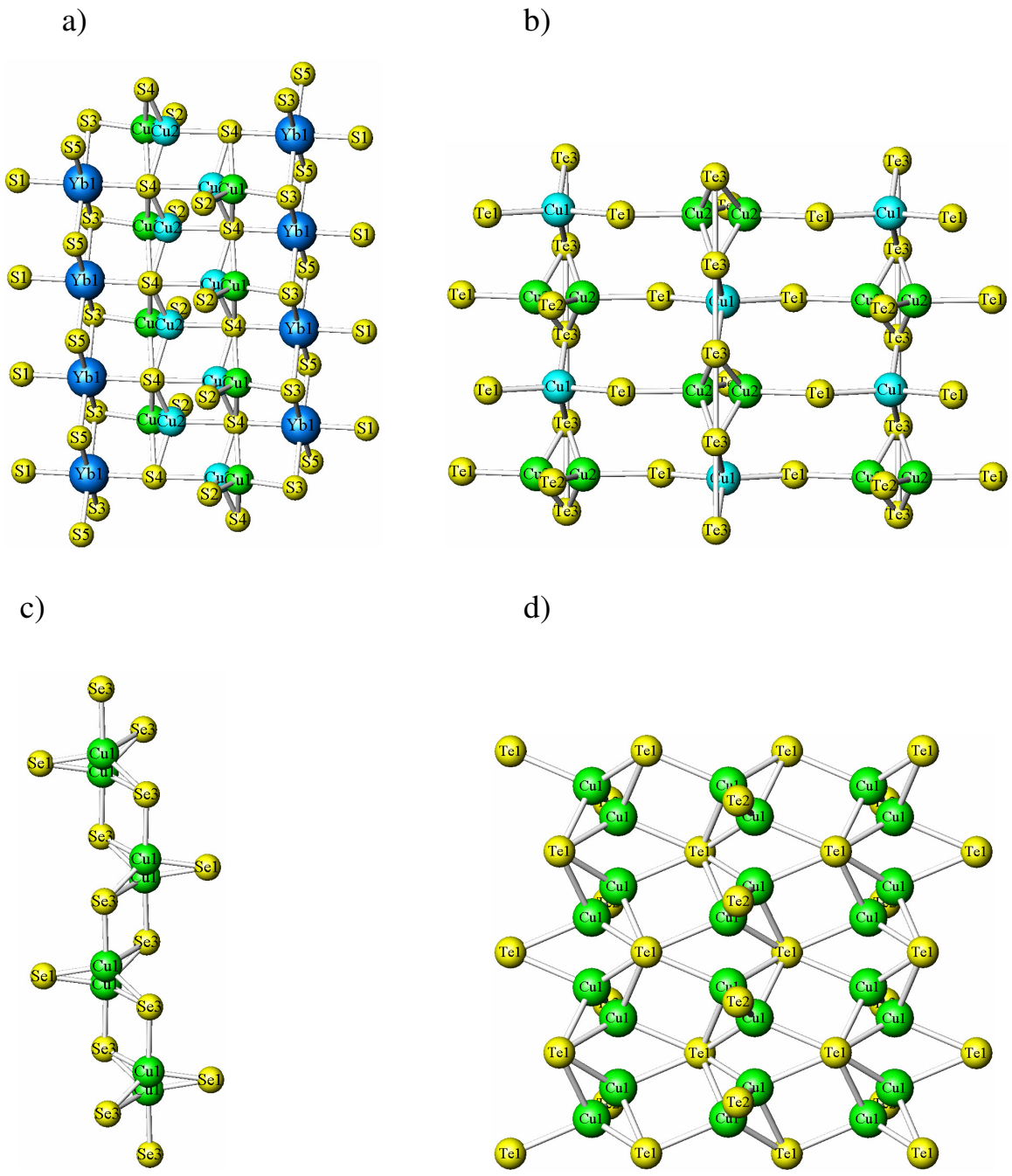

Figure 3

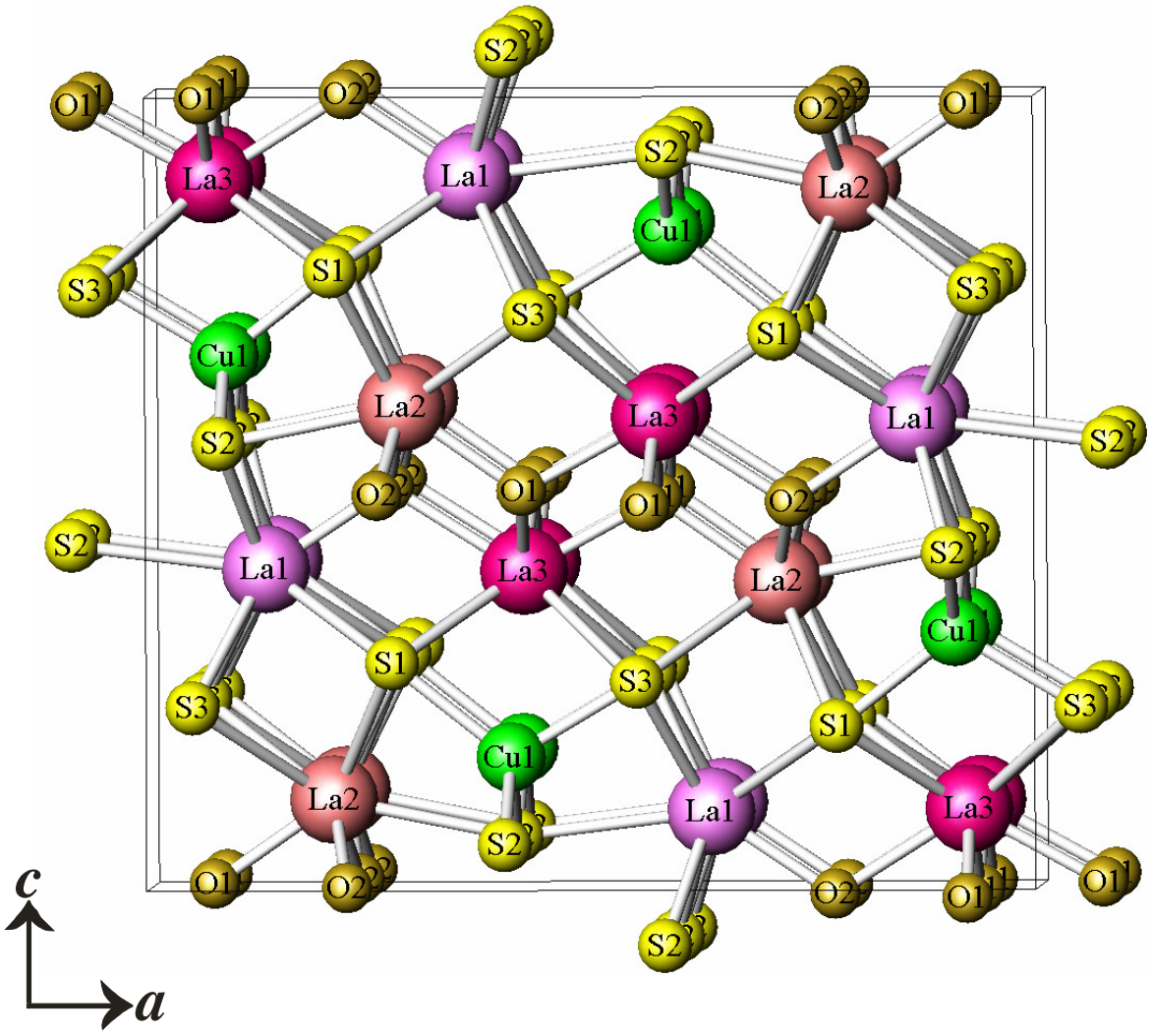
S2
O1
O1
O2
O2
O1
La3
La1
S2
La2
Cu1
S1
S3
S3
S1
S3
Cu1
La2
La3
La1
S2
S2
O2
O1
O1
O2
S2
S2
La1
La3
La2
S2
Cu1
S1
S3
S3
S1
S3
Cu1
La2
La1
La3
S2
O1
O2
O2
O1
O1
S2
c
a

Figure 4

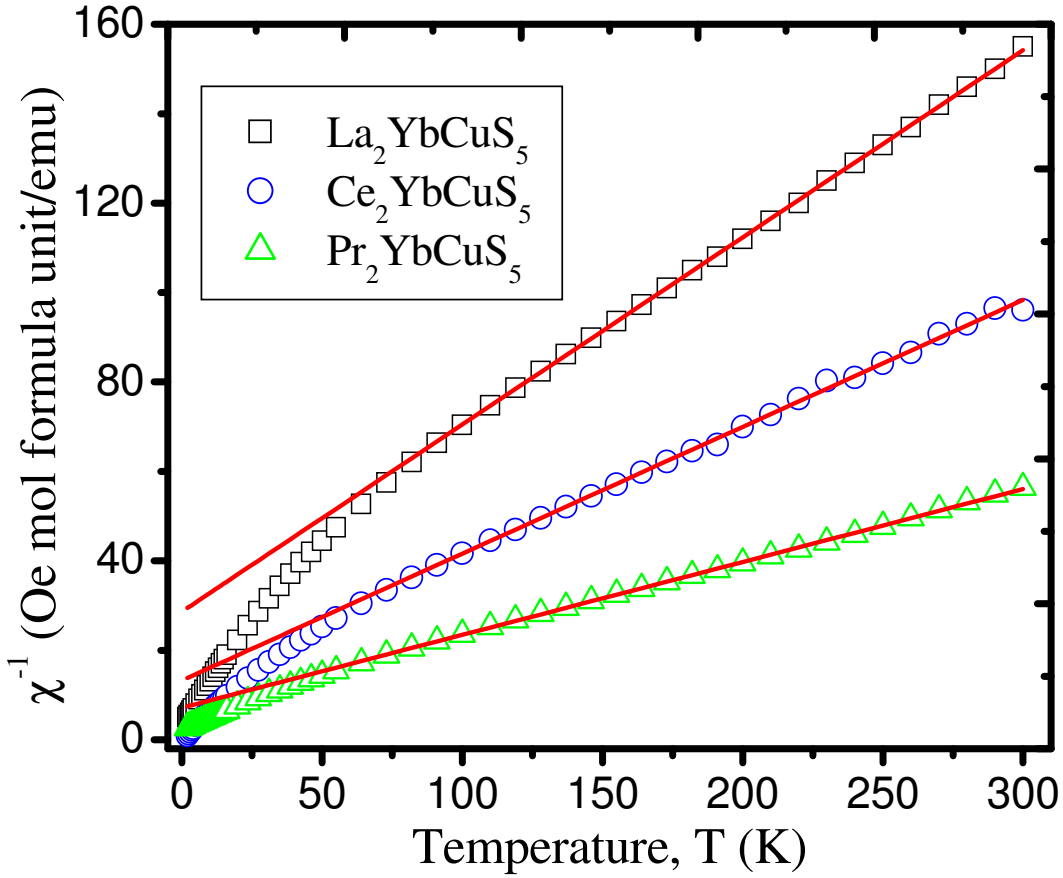
160
120
80
40
0
0
50
100
150
200
250
300
Temperature, T (K)
χ-1 (Oe mol formula unit/emu)
La2YbCuS5
Ce2YbCuS5
Pr2YbCuS5

Figure 5

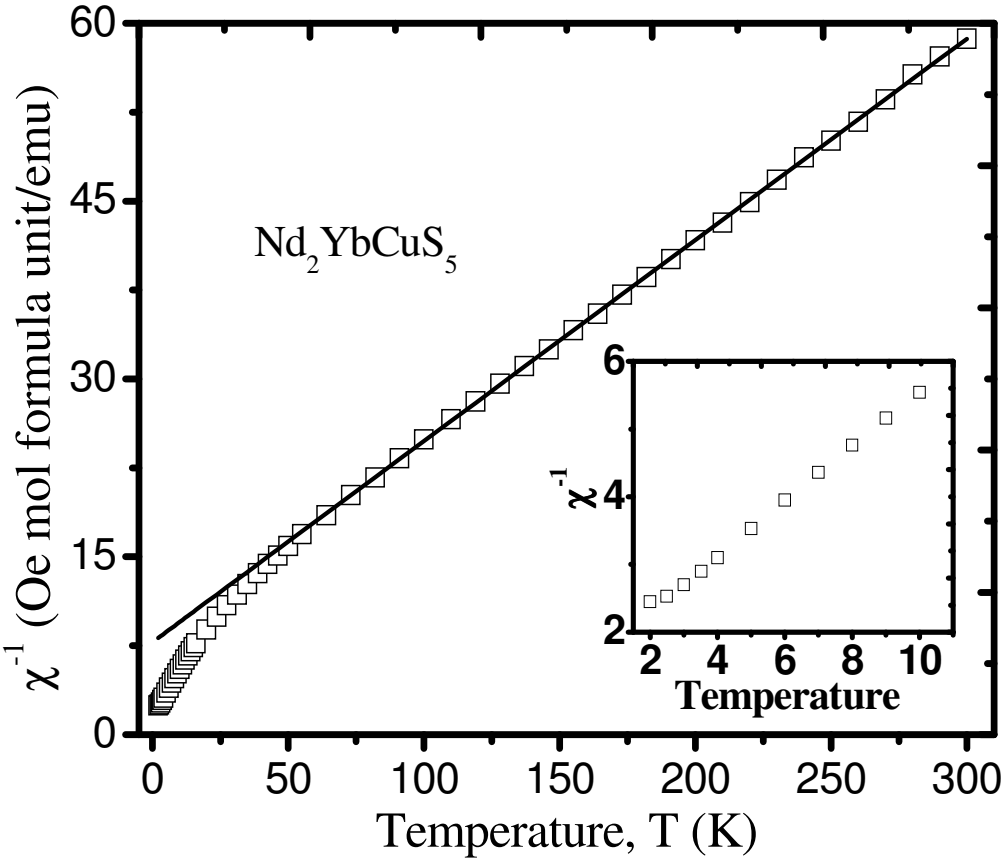
60
45
30
15
0
χ^{-1} (Oe mol formula unit/emu)
Nd_2YbCuS_5
0
50
100
150
200
250
300
Temperature, T (K)
6
4
2
χ^{-1}
2
4
6
8
10
Temperature

Figure 6

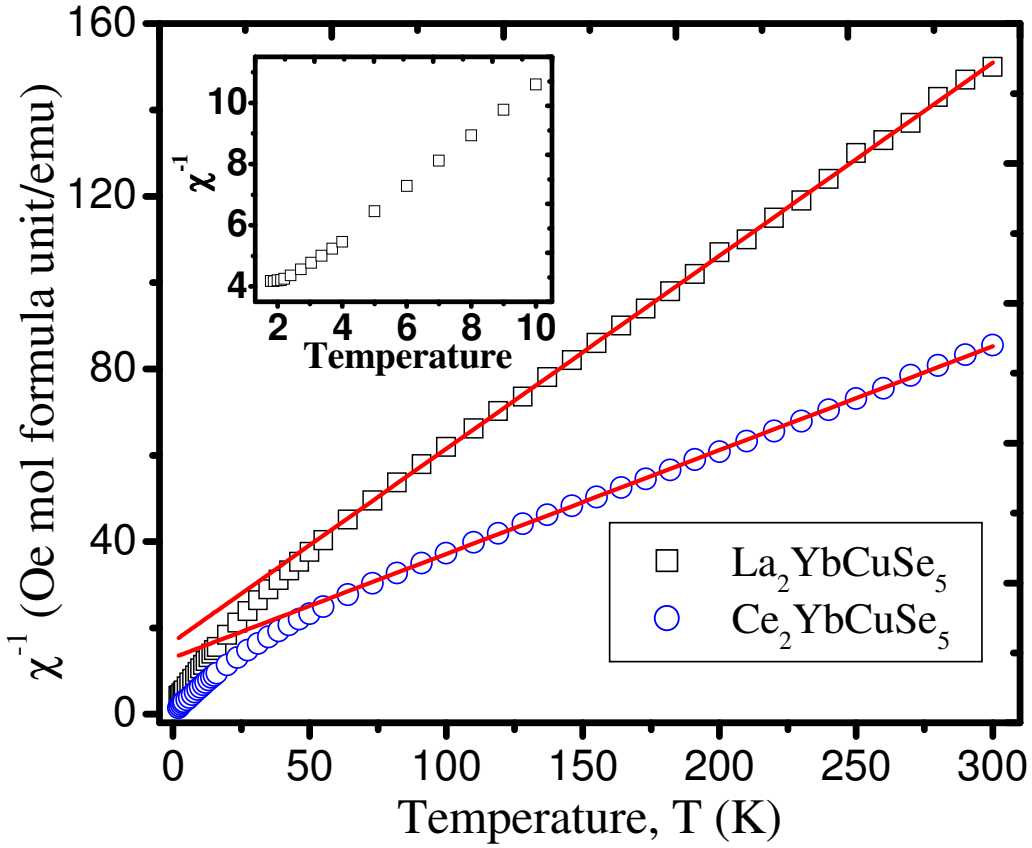
160
120
80
40
0
χ-1 (Oe mol formula unit/emu)
0
50
100
150
200
250
300
Temperature, T (K)
La2YbCuSe5
Ce2YbCuSe5
χ-1
10
8
6
4
2
4
6
8
10
Temperature

Figure 7

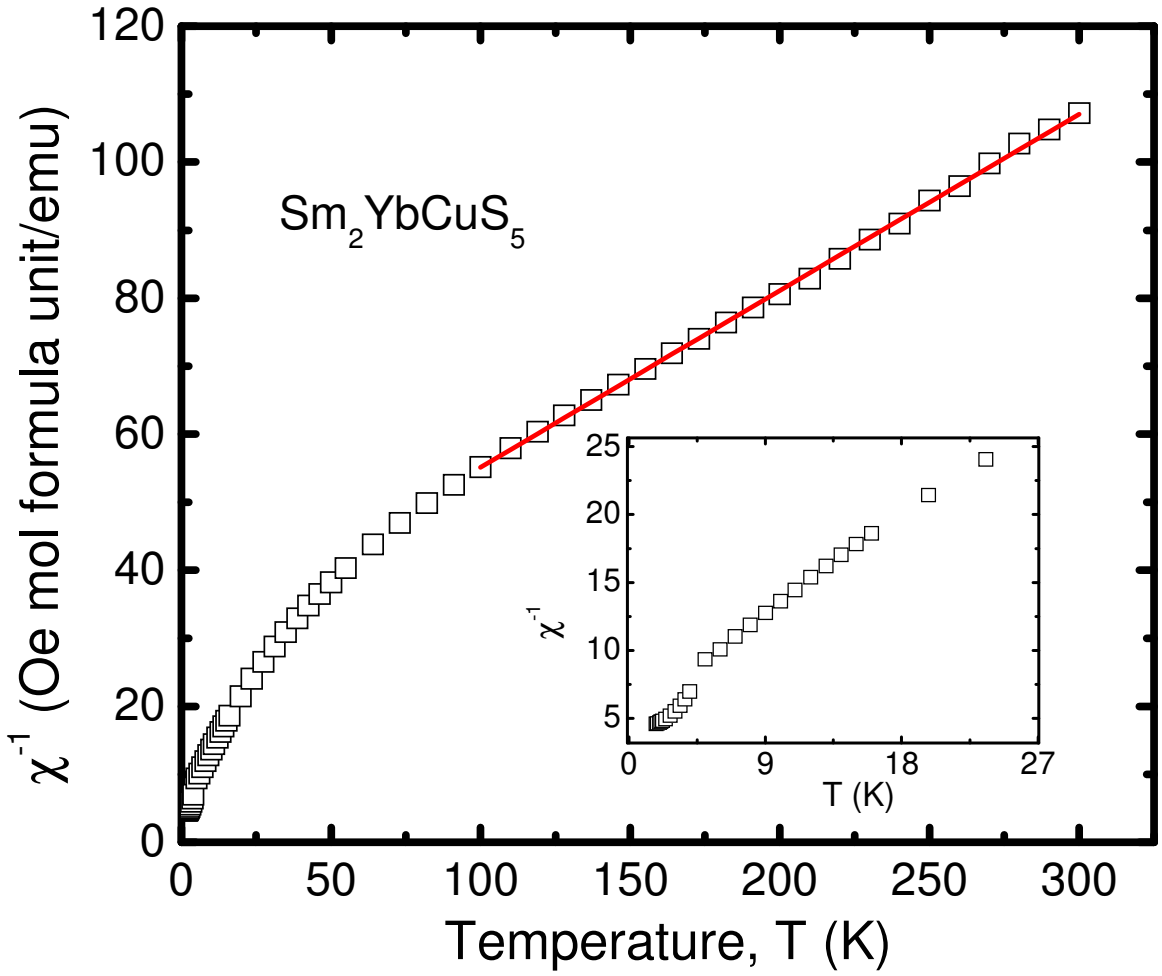
120
100
80
60
40
20
0
χ^{-1} (Oe mol formula unit/emu)
Sm_2YbCuS_5
0
50
100
150
200
250
300
Temperature, T (K)
25
20
15
10
5
χ^{-1}
0
9
18
27
T (K)

Figure 8

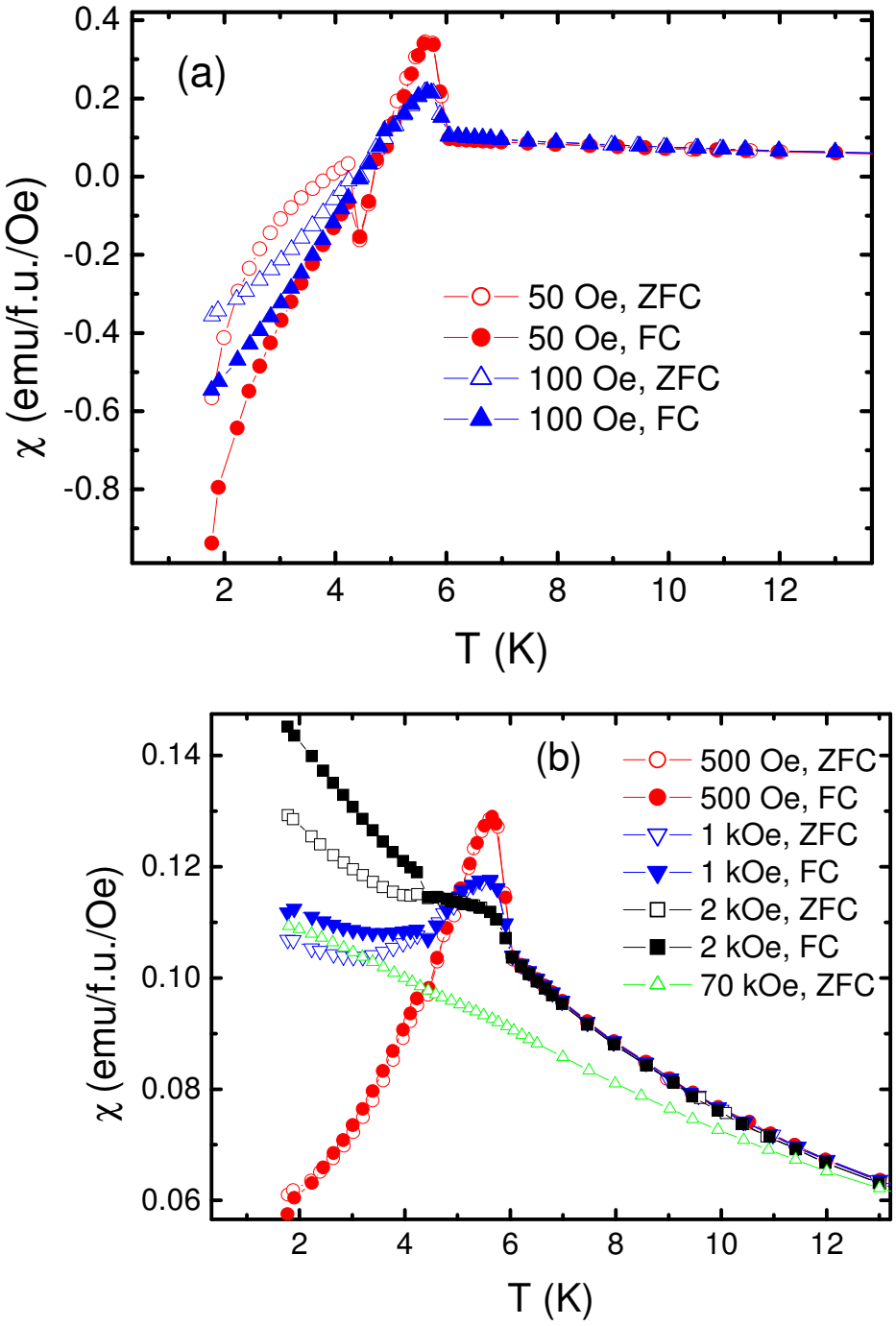
(a)
50 Oe, ZFC
50 Oe, FC
100 Oe, ZFC
100 Oe, FC
χ (emu/f.u./Oe)
T (K)
(b)
500 Oe, ZFC
500 Oe, FC
1 kOe, ZFC
1 kOe, FC
2 kOe, ZFC
2 kOe, FC
70 kOe, ZFC
χ (emu/f.u./Oe)
T (K)

Figure 9

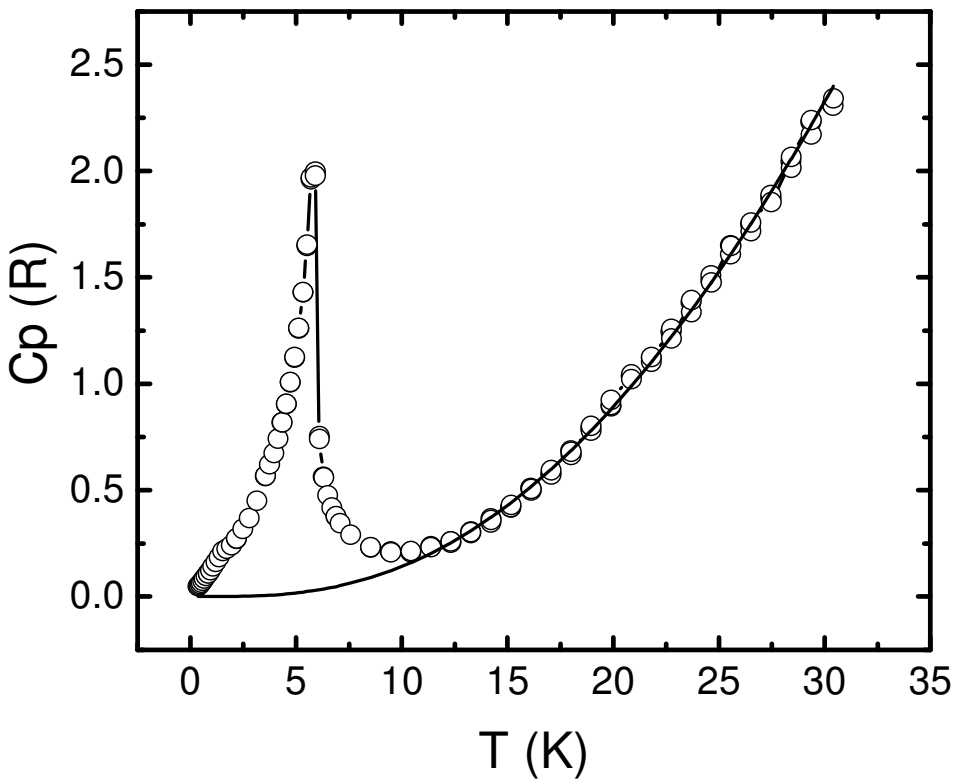

Figure 10

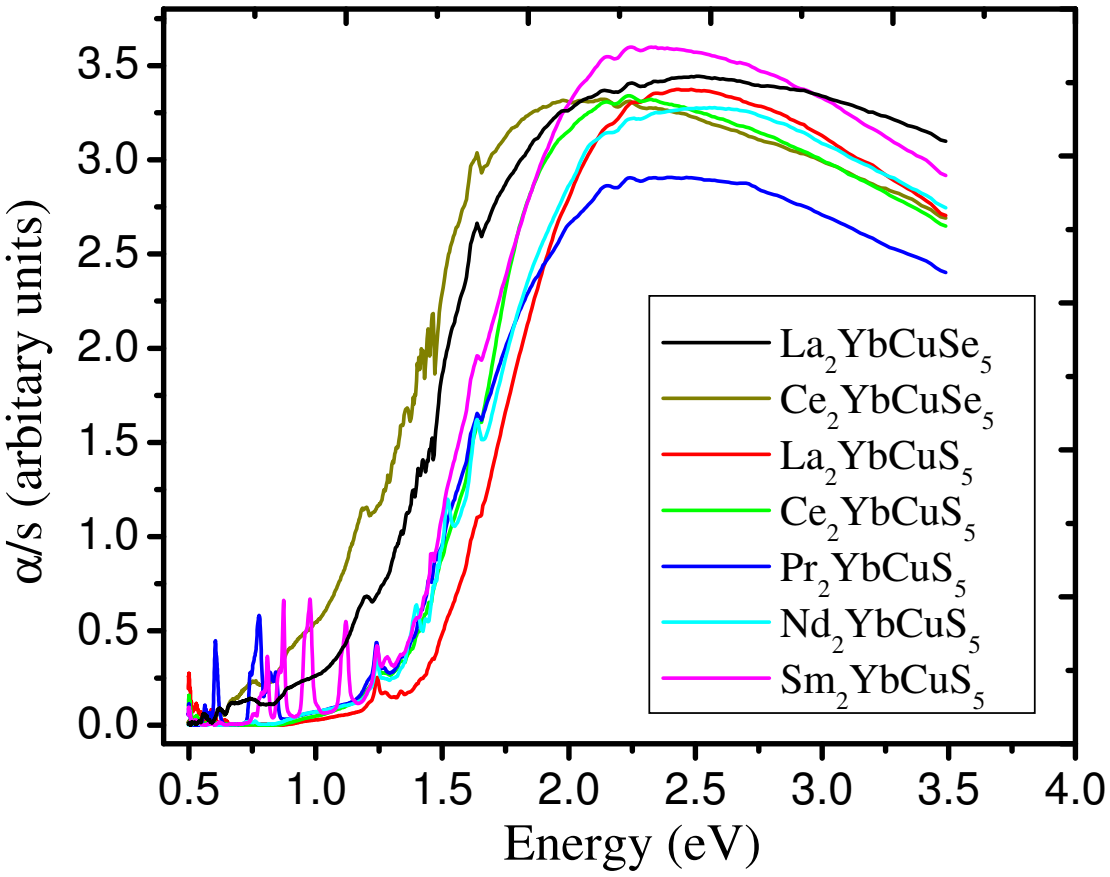
α/s (arbitary units)
Energy (eV)
0.0
0.5
1.0
1.5
2.0
2.5
3.0
3.5
4.0
La2YbCuSe5
Ce2YbCuSe5
La2YbCuS5
Ce2YbCuS5
Pr2YbCuS5
Nd2YbCuS5
Sm2YbCuS5

Figure 11

DISCLAIMER